REPORT DOCUMENTATION PAGE

Form Approved
OMB NO. 0704-0188

1. AGENCY USE ONLY (Leave Blank)	2. REPORT DATE	3. REPORT TYPE AND DATES COVERED
	4/17/2010	new reprint

4. TITLE AND SUBTITLE
Combustion synthesis of metallic foams from nanocomposite reactants

5. FUNDING NUMBERS
W911NF-04-1-0217

6. AUTHOR(S)
EM Hunt, ML Pantoya, RJ Jouet

7. PERFORMING ORGANIZATION NAME(S) AND ADDRESS(ES)
Texas Tech University, Mechanical Engineering Department, Lubbock, TX 79409

8. PERFORMING ORGANIZATION REPORT NUMBER

9. SPONSORING / MONITORING AGENCY NAME(S) AND ADDRESS(ES)
U. S. Army Research Office
P.O. Box 12211
Research Triangle Park, NC 27709-2211

10. SPONSORING / MONITORING AGENCY REPORT NUMBER

11. SUPPLEMENTARY NOTES
The views, opinions and/or findings contained in this report are those of the author(s) and should not be construed as an official Department of the Army position, policy or decision, unless so designated by other documentation.

12 a. DISTRIBUTION / AVAILABILITY STATEMENT
Approved for public release;federal purpose rights

12 b. DISTRIBUTION CODE

13. ABSTRACT (Maximum 200 words)

Highly porous intermetallic alloys were created through self-propagating high-temperature synthesis. The reactants are composed of nano-scale particles of nickel (Ni), micron-scale particles of aluminum (Al), and nano-scale Al particles passivated with a gasifying agent, C13F27COOH. The concentration of nano-Al particles present in the reactant matrix was controlled according to the wt % gasifying agent. Flame propagation was observed to transition from normal to convectively dominant burning as more gasifying agent became present in the reactants. Ignition delay times were reduced by two orders of magnitude when only 2.24 wt % nm Al particles were present. The product alloy expanded by a factor of 14 in the axial direction with 1.6 wt % nm Al (corresponding to 10 wt % gasifying agent). The total porosity of the pellets increased with increasing nano-Al concentration.

14. SUBJECT TERMS	15. NUMBER OF PAGES
reaction synthesis, nickel aluminides, NiAl, combustion syntehsis, metallic foams	10
	16. PRICE CODE

17. SECURITY CLASSIFICATION OR REPORT	18. SECURITY CLASSIFICATION ON THIS PAGE	19. SECURITY CLASSIFICATION OF ABSTRACT	20. LIMITATION OF ABSTRACT
UNCLASSIFIED	UNCLASSIFIED	UNCLASSIFIED	U

Enclosure 1

Available online at www.sciencedirect.com
SCIENCE DIRECT
Intermetallics 14 (2006) 620–629
Intermetallics
www.elsevier.com/locate/intermet

Combustion synthesis of metallic foams from nanocomposite reactants

Emily M. Hunt [a], Michelle L. Pantoya [a,*], R. Jason Jouet [b]

[a] Department of Mechanical Engineering, Texas Tech University, Lubbock, TX 79409, USA
[b] Research and Technology Department, Indian Head Division-Naval Surface Warfare Center, Indian Head, MD 20640, USA

Received 12 March 2005; accepted 24 October 2005
Available online 4 January 2006

Abstract

Highly porous intermetallic alloys were created through self-propagating high-temperature synthesis. The reactants are composed of nano-scale particles of nickel (Ni), micron-scale particles of aluminum (Al), and nano-scale Al particles passivated with a gasifying agent, $C_{13}F_{27}COOH$. The concentration of nano-Al particles present in the reactant matrix was controlled according to the wt% gasifying agent. Flame propagation was observed to transition from normal to convectively dominant burning as more gasifying agent became present in the reactants. Ignition delay times were reduced by two orders of magnitude when only 2.24 wt% nm Al particles were present. The product alloy expanded by a factor of 14 in the axial direction with 1.6 wt% nm Al (corresponding to 10 wt% gasifying agent). The total porosity of the pellets increased by a factor of 8 (i.e., from 10 to 80% porosity for 0–14 wt% gasifying agent).

Keywords: A. Nickel aluminides based on NiAl; A. Nanostructured intermetallics; C. Reaction synthesis

1. Introduction

Heat insulating materials can be distinguished by their high porosity which significantly lowers their thermal conductivity and improves the material's resistance to heat energy transport. These materials are used in various sectors of industry to reduce heat losses and lead to saving fuel and energy [1,2]. In chemistry, highly porous materials are used to aid catalytic processes [3,4]. In biology, highly porous materials are used as bone replacements [5,6]. Porous bioactive materials are implanted in bone and have been shown to activate a biologic response that enhances bone healing [5,6]. The multitude of applications for highly porous materials has spurred interest in material scientists to explore various synthesis methods and generate a variety of highly porous alloys, ceramics, intermetallics and cermet materials.

One goal of this study is to generate highly porous metallic foams using nanoparticle reactants through the chemical process of Self-propagating High-temperature Synthesis (SHS). This technique has been used, before [7–9] and was chosen based on two potential advantages SHS offers over other synthesis techniques. The first is that the reaction can take place without the need of an additional or external oxidizer, such as ambient air. The reactants are an energetic composite of fuel and oxidizer particles such that the reactions can occur in a vacuum (e.g. outer space) or underwater. The second advantage pertains to the advancements in nanotechnology that have enabled the production of nano-scale particles with unique chemical and physical properties, such as reduced melting temperatures [10], higher surface energy [11] and distinctive absorption properties when compared to traditional micron-scale particles [12]. These properties can be exploited during the SHS process to synthesize highly porous intermetallic alloys.

An SHS reaction tailored for the generation of a highly porous material can be described by the general formula in Eq. (1).

$$A + B + G \rightarrow P + G' \quad (1)$$

where A is a metallic fuel (e.g. aluminum), B is a metal or nonmetallic oxidizer (e.g. Ni or Fe_2O_3, respectively) and G is a gasifying or blowing agent (e.g. Teflon [13], sodium tetraborate or borax [14]). On the product side of the reaction, P represents a solid product (e.g. carbides, silicides, intermetallics [15]) and G' designates product off gasses that result from reactions with the gasifying agent.

The reactants are homogeneously mixed and pressed into a cylindrical pellet. Combustion synthesis can be initiated on the sample surface by a chemical, electrical, mechanical or a

* Corresponding author. Tel.: +1 806 742 2452; fax: +1 806 742 3540.
E-mail address: michelle.pantoya@coe.ttu.edu (M.L. Pantoya).

0966-9795/$ - see front matter © 2005 Elsevier Ltd. All rights reserved.
doi:10.1016/j.intermet.2005.10.011

radiant energy source (e.g. laser ignition). One advantage of nanoparticle composites is their heightened sensitivity to ignition. For example, incorporating nano-Al particles into the reactant matrix has been shown to reduce the ignition delay time [16] and activation energy [17]. Nanoparticles thereby increase the efficiency and cost effectiveness of the SHS process by reducing the energy required to initiate the reaction. Once initiated, the reaction will be self-sustaining through the sample if the adiabatic flame temperature for the reaction is greater than or equal to approximately 2000 K [18].

The porous nature of the product mainly results from outgassing of the gasifying agent during the reaction. Without a gasifying agent, the starting porosity of the sample is a strong function of the bulk density of the pellet. Merzhanov et al. [19] showed SHS can be used to produce ceramic and cermet materials with a total porosity of 30–50%. Shteinberg et al. [20] showed that by using sodium tetraborate ($Na_2B_4O_7 \cdot 10H_2O$) as a gasifying agent the gases formed in the combustion wave increased the volume of porous titanium carbide ($TiC_{0.6}$) by a factor of 3–5, with a total porosity up to 85%.

In previous combustion synthesis studies, the gasifying agent is added as a separate reactant and usually in the form of a powder or granular material [13,20]. Also, previous work pertaining to the synthesis of porous materials using SHS was limited to micron-scale reactant particles because nano-scale particles have only recently become available. In a recent study, nano-scale Al particles replaced micron-scale Al particles in the SHS of NiAl [16]. The NiAl alloy synthesized was suggested to have inferior structural properties compared with micron-scale composites. Hunt et al. [16] attributed this result to excessive concentrations of Al_2O_3 inherent as a passivation shell in the nm Al reactant particles. When the particle diameter approaches the nano-scale the surface area to volume ratio increases dramatically and the overall percent of Al_2O_3 present in the powder can become appreciable. For example, Granier and Pantoya [21] reported that nano-Al particles can consist of up to 62% Al_2O_3 while micron-scale Al particles can contain less than 1% Al_2O_3. Excessive concentrations of Al_2O_3 act as a heat sink during the combustion process, retard flame propagation and can lead to incomplete combustion [16,21]. Granier et al. [22] showed that small amounts of Al_2O_3 (i.e., roughly 5 wt%) can actually strengthen the synthesized alloy by increasing the materials resistance to wear. This interesting study showed that adding only a small amount of nano-scale Al particles to a micron-scale Al and Ni reaction optimized the combustion performance and macroscopic properties of the alloy by (1) reducing the ignition energy; and (2) producing a product with improved tribology properties that could otherwise not be attained by using strictly nano- or micron-scale Al particles.

In more recent work, Jouet et al. [23] introduced nano-Al particles passivated with a perfluoroalkyl carboxylic acid ($C_{13}F_{27}COOH$) rather than Al_2O_3. The surface passivation of the oxide-free Al nanoparticles was accomplished using self assembled monolayers via a wet chemistry technique such that the particles are prepared and coated in solution and have a monolayer of carboxylic acid passivation. The resulting composite particles are on the order of 20–200 nm in diameter and contain ~15% Al by mass with the remaining concentration composed almost entirely of $C_{13}F_{27}COOH$ [23]. The high concentrations of carbon and fluorine in this new passivation layer allow for significant gaseous product formation upon combustion. The perfluoroorganic moiety can therefore act as a gasifying agent during the combustion synthesis process. Additionally, the perfluoroorganic carboxylate species may act as a fluxing agent with the micron size Al particles present. In this capacity, the fluorine reacts with the surface Al_2O_3 of the larger Al particles. Ignition time would be reduced for the micron size Al particles in this scenario, but perhaps more importantly, volatile Al–F–O species would be formed aiding in material gasification/expansion.

Based on the results obtained when micron-Al particles were incrementally replaced with nano-Al particles [22] coupled with the latest developments in nano-Al particle technology described in [23], this study examines the creation of a porous metallic material produced from nano-scale Ni particles combined with micron-scale particles of Al which are incrementally replaced with nano-scale Al particles passivated with $C_{13}F_{27}COOH$. The $C_{13}F_{27}COOH$ passivation of the nano-Al particles plays an important role in this reaction by acting as a gasifying agent thereby increasing the pressure in the nano-pores during combustion and affecting the microstructure of the final product.

This study is unique because it not only examines the SHS of a porous metallic foam using nano-particle reactants (which to the authors' knowledge has not previously been investigated), but also incorporates a gasifying agent as an intrinsic part of the nano-scale particle rather than as a discrete additive in the form of a powder or granular material. The fact that the gasifying agent encapsulates the nano-scale Al media will improve the homogeneity of the mixture by more precisely controlling the diffusion distance between gasifying agent and other metallic reactants.

The overall objective of this study is to examine the role of nano-scale reactant particles of Ni and Al passivated with $C_{13}F_{27}COOH$ in the production of a highly-porous metallic alloy. This objective will be accomplished by examining combustion behaviors such as ignition delay time and combustion velocity as a function of gasifying agent and evaluating the effect of the gasifying agent content on the microstructure of the final product. In particular, when a large amount of pore forming additive is introduced, the continuity of the sample may be violated and the sample itself may not have enough structural stability to maintain a continuous shape. Determining this critical limit for the additive is a goal of this work. Before reaching this critical limit, the synthesis process will effectively increase porosity, reduce density, and increase volumetric expansion in the final product. Combustion behaviors will be observed by igniting one end of the pellet with a CO_2 laser, examining flame propagation with a high-speed camera and measuring ignition and reaction temperatures using micro-thermocouples. Measurements of ignition delay time, temperature and flame propagation behavior will be correlated with the product microstructure.

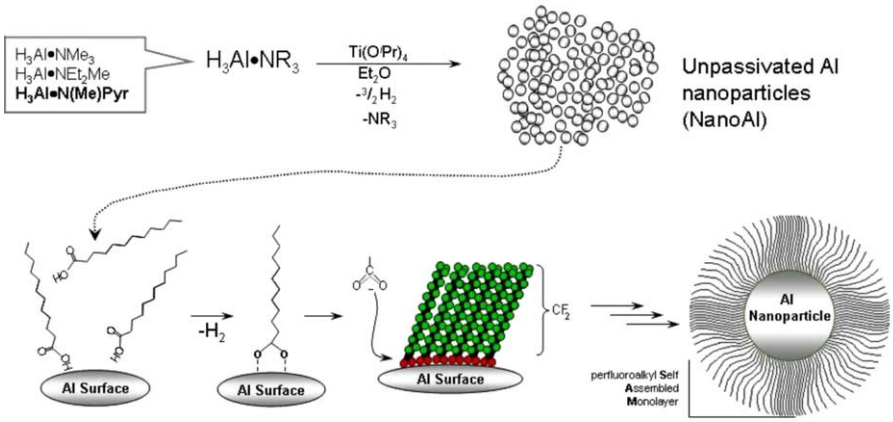

Fig. 1. Schematic diagram illustrating bonding between passivation chain and Al particle surface.

2. Experimental

2.1. Self-assembled monolayer (SAM) passivation of nano-Al particles

Nanoscale Al particles were synthesized at Indian Head Division, Naval Surface Warfare Center (IHDNSWC). The oxide free Al particles were synthesized in solution by catalytic decomposition and coated in situ using a perfluoroalkyl carboxylic acid SAM (Self Assembled Monolayers) [23]. Because the Al particles are synthesized using wet chemistry techniques and coated in solution, they have a monolayer of carboxylic acid passivation. This SAM coating passivates the aluminum and prevents the oxidation of the particles in air [23].

The nano-Al/$C_{13}F_{27}COOH$ composites were developed by passivation of the surface of bare Al nanoparticles using perfluorotetradecanoic acid, $C_{13}F_{27}COOH$. The authors [23] showed that the carboxylic acid binds to the surface of the Al particle through the COOH functionality forming an aluminum carboxylate moiety and leaving the perfluorinated carbon chain intact. The resulting particles are thus comprised of an Al center core with covalently bonded perfluorinated alkyl species coating the surface, as illustrated in Fig. 1.

Scanning electron microscopy images (SEM) of the nano Al/$C_{13}F_{27}COOH$ composite were limited because extreme magnification results in charging which prevents or diminishes image resolution. Additionally, particles appeared to vaporize under extreme magnification. Acceptable images were obtained at 200 kV magnification using a LEO scanning electron microscope at the National Research Laboratory. Fig. 2 shows particles on the order of 20–200 nm in diameter. Additional characterization of these particles has been performed and reported elsewhere [23]. For example, based on thermogravimetric analysis (TGA), Jouet et al. [23] showed that the active Al content (i.e. weight percent of material that is actually Al) is roughly 15%.

2.2. Sample preparation and experimental setup

The initial mixtures were composed of 4 μm Al particles, 800 nm Ni particles, and $C_{13}F_{27}COOH$ coated nano-scale Al particles that varied between 0 and 2.56 wt% content (corresponding to a variation in gasifying agent (GA) content between 0 and 16 wt%). The distribution of active Al by composition is illustrated in Fig. 3. Ten mixtures of Al/Al–$C_{13}F_{27}COOH$/Ni were prepared, each with a varying distribution of Al particle size ranging from 0 to 2.56 wt% nm Al. The overall mixture was maintained at a 1:1 molar ratio of Ni:Al. This mixture ratio was shown to be optimum for producing a product with the highest content of NiAl and optimum wear properties [24].

The reactant particles were suspended in a solvent of hexanes and mixed using ultrasonic waves that break up macro-scale agglomerates. The final powder mixture was dried and cold-pressed in a uniaxial die to create cylindrical pellets with a diameter of approximately 6.5 mm and initial length of 1 mm. The theoretical maximum density was calculated for each mixture as a weighted average of the pure solid densities of the three constituent reactants (Al, Ni and $C_{13}F_{27}COOH$). Each sample was pressed to a density of 70% of the theoretical value.

For each sample set illustrated in Fig. 3, six pellets were pressed and examined for ignition delay time, temperature and combustion velocity. The front face of each pellet was coated with a flat black paint to eliminate scattering of the laser light due to a high surface reflectivity. Micro-thermocouples were used to measure ignition temperatures and were fixed in spring tension along the pellet's front face. The thermocouples were

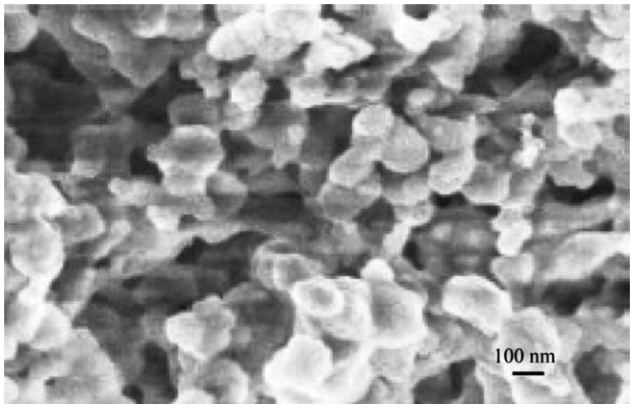

Fig. 2. SEM image of nano-scale Al particles passivated with $C_{13}F_{27}COOH$.

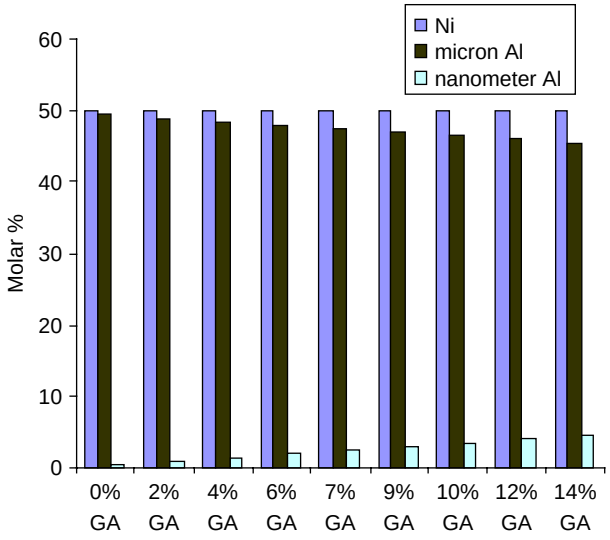

Fig. 3. Schematic showing molar percent mixture ratios of Ni, μm Al and nm Al as a function of the weight percent of gasifying agent (GA).

50-μm C-type tungsten–rhenium with a response time of 50 ms. The thermocouple voltages were recorded using an INET (model 100, Omega) data acquisition system in oscilloscope mode with a 10-bit 80 mV range and 62 kHz sample rate for each channel.

A schematic of the experimental setup is shown in Fig. 4. The pellets were ignited with a 50 W CO_2 laser (Universal Laser Systems Inc., Scottsdale, AZ). A power meter and associated optics were used to monitor the laser power and align the laser beam with the front face of the pellet, respectively. Ignition and flame propagation were recorded using a Phantom IV (Vision Research, Wayne, NJ) high-speed camera, which captures images at 32,000 frames per second (fps). The reaction was viewed perpendicular to the direction of flame propagation (Fig. 4). Further details of this experimental apparatus are discussed elsewhere [16].

Ignition delay time was measured based on the 'first-light' approach in which ignition time is determined as the time lapse between sample exposure to the laser beam and detection of the first light using the high-speed camera operating at 32,000 fps. This may not guarantee ignition but is a commonly used technique for experimentally determining ignition times. The high speed camera is synchronized with the CO_2 laser and detects light intensity. In this way, the reaction light is used as the illuminating source to visualize the ignition process.

Flame propagation was observed using neutral density filters on the Phantom IV camera to reduce the intensity of the light emitted from the reaction and eliminate image saturation. In this arrangement, neutral density filters were used to limit the light transmission to 2.5%. The combustion velocity was calculated using the 'track edge' feature from the Vision Research image processing software compatible with the Phantom IV.

The product microstructure was examined with a scanning electron microscope (SEM-Hitachi S-570) using a high-resolution stage at a voltage of 15 kV. The porosity of the products was measured by Porous Materials, Inc. (PMI) (Ithaca, NY) with a mercury pycnometry using silwick as the wetting agent, which is a method analogous to hydrostatic weighing. Measurements were also made based on still frame images of the pellets before and after self-propagation of the reaction to determine radial and axial elongation.

3. Results

3.1. Ignition delay time

Fig. 5 shows the ignition time as a function of nm Al particle content and corresponding GA content. The bars in Fig. 5 represent the standard deviations in the measurements determined by repeated measurements for at least six samples. The ignition time decreases as nm Al content increases.

Fig. 6 shows the average ignition temperature and standard deviation as a function of nm Al and GA content. The ignition temperature decreases below the bulk melting temperature of Al (shown in Fig. 6 at 660 °C) when at least 6 wt% $C_{13}F_{27}COOH$ is added to the mixture. Thermocouple measurements for pellets exceeding 10% GA content could not be accurately realized because ignition delay times are on the order of the thermocouple response time creating excessive uncertainty in the temperature measurements.

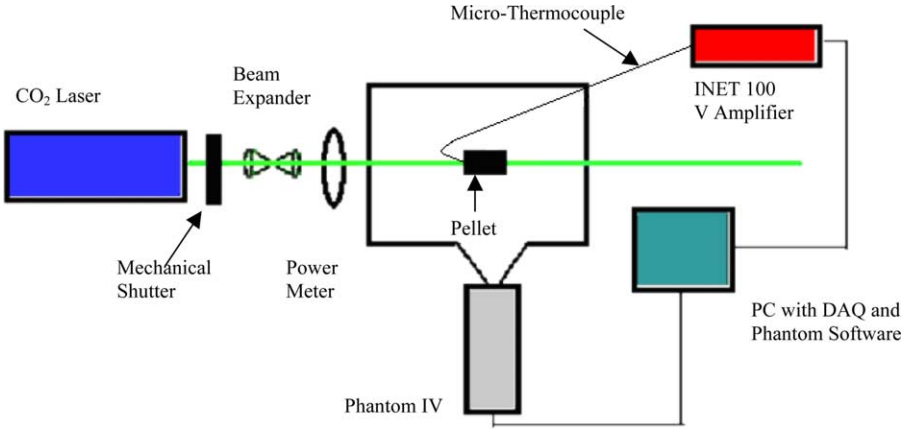

Fig. 4. Experimental setup including laser ignition source, pellet, high-speed camera, data acquisition system (DAQ) and micro-thermocouple.

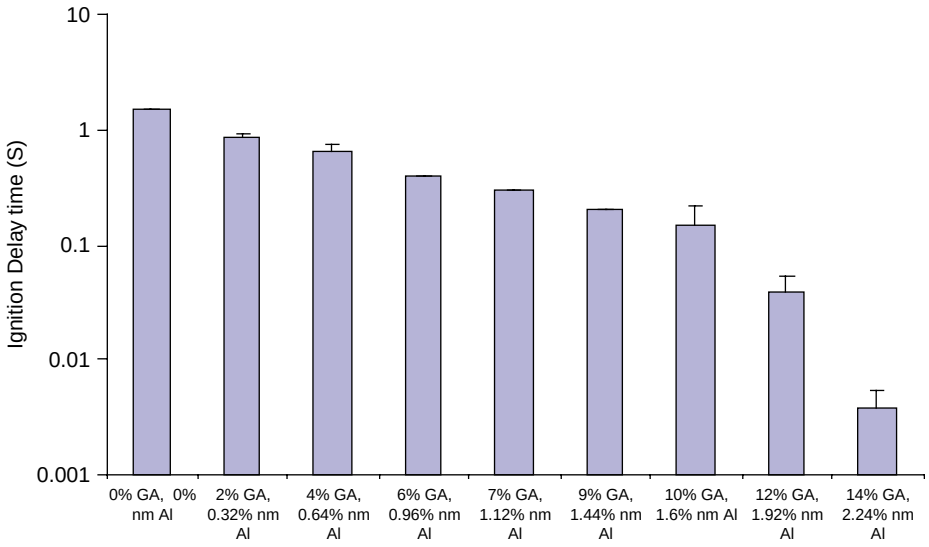

Fig. 5. Ignition time as a function of the wt% gasifying agent (GA) and corresponding wt% nano Al content.

3.2. Combustion velocity

The combustion velocity is reported as a function of nm Al and GA content in Table 1 and increases from roughly 0.007–0.7 m/s with nm Al content. The most interesting behavior occurs at 7% GA: adding the first 7% GA leads to a bare doubling of velocity, whereas each additional 2% doubles the velocity. A similar increase in velocity was previously observed in porous explosive charges and attributed to a transition from normal diffusive to convective burning [25]. When convective burning takes precedence over thermal conduction and radiation, energy and mass transfer in the burning zone are driven by gas jets that penetrate into the pores of the energetic material. Bobolev et al. [25] explain that in some cases penetration of combustion into the pores is followed by the establishment of a stationary convective burning regime whose rate substantially exceeds the normal burning rate. In an effort to identify this burning regime, an analysis of porous energetic material combustion under constant pressure conditions has lead to a stability criterion known as the Andreev number, *An* (Eq. (2)) [25]. This non-dimensional parameter is similar to the Peclet number except tailored for reacting flow through porous media.

$$An = \frac{\rho_b U d_h c_p}{k_g} = \text{const.} \tag{2}$$

In this equation, ρ_b is the bulk density of the composite, U is the measured combustion velocity, d_h is the hydraulic pore diameter, c_p is the heat capacity of the composite and k_g is the thermal conductivity of the gas. If this value exceeds a certain constant, combustion penetrates into the porous structure and convective mechanisms dominate flame propagation. In making this calculation it is necessary to estimate the characteristic pore size which is defined as the hydraulic pore diameter, d_h, given from Eq. (3) [26].

$$d_h = \frac{4\varepsilon}{A_o(1-\varepsilon)} \tag{3}$$

In this equation ε is the void volume, A_o is the specific surface area based on the solid volume and is calculated as the solid surface area divided by the solid volume (A_s/V_s), and $(1-\varepsilon)$ is the solid volume fraction [26].

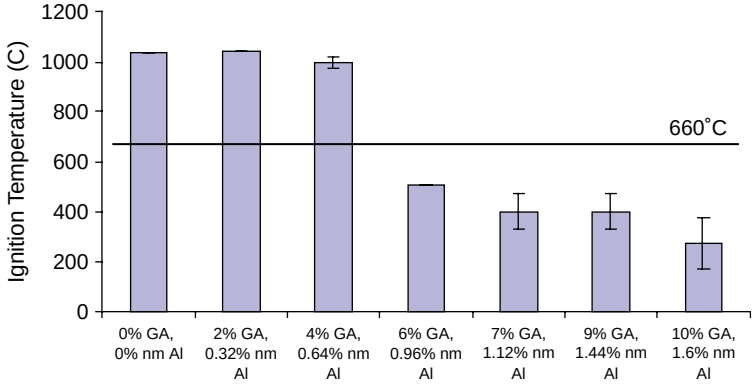

Fig. 6. Ignition temperature as a function of the wt% gasifying agent (GA) and corresponding wt% nano Al content.

Table 1
Calculated thermal and physical parameters for all Ni–Al–$C_{13}F_{27}COOH$ composites

% GA	% nm Al	ε	Combustion velocity (m/s)	Hydraulic pore diameter (m)	Andreev number
0	0	9.56	0.007	2.281×10^{-4}	0.03
2	0.32	32.85	0.007	7.840×10^{-4}	0.09
4	0.64	37.75	0.009	9.009×10^{-4}	0.14
7	1.12	34.31	0.013	8.189×10^{-4}	0.18
9	1.44	35.00	0.031	8.189×10^{-4}	0.43
10	1.60	35.48	0.061	8.467×10^{-4}	0.88
12	1.92	40.38	0.136	9.636×10^{-4}	2.23
14	2.24	44.80	0.313	1.069×10^{-3}	5.69
16	2.56	47.78	0.700	1.140×10^{-3}	13.58

Table 1 shows the calculated values for the Andreev numbers as well as the measured combustion velocities and calculated void volume and pore size. These calculations are based on the assumption of k_g is 0.137 W/m K corresponding to air at an average temperature of 2000 K. All samples have a density of 4140 kg/m^3, a heat capacity of 673 J/kg K and a specific surface area (A_o) of 5966 m^{-1}.

Bobolev et al. [25] calculated critical *An* numbers between 3 and 10 and generalized that if the $An>6$ combustion will penetrate into the pores and convective mechanisms will play the primary role in accelerating the flame front. Table 1 shows the critical Andreev number in which the flame propagation transitions from normal burning to convective burning is roughly 0.18. This analysis suggests that the transition from low to high combustion velocities results in a shift in the flame propagation mechanism. The When $An<0.18$, the flame is propagating under normal diffusive burning conditions. However, when $An>0.18$, the mechanism for propagation is controlled by convection. This condition is observed at 16 wt% gasifying agent, where the pellet cannot maintain its original structure and is blown apart by the convective forces dominating the reaction.

3.3. Porosity and microstructure of the products

Fig. 7 shows porosity of the product without nm Al reactant particles is 16%. As the nm Al content added to the reactants increases, the porosity continues to increase until 14 wt% $C_{13}F_{27}COOH$ where the porosity reaches almost 80% (Fig. 7).

Fig. 8 shows a pellet containing 7 wt% GA that expands from 1 to 7 mm during combustion. The relative elongation with respect to GA and nm Al content is shown in Fig. 9. It is noted that at 12 and 14% GA the structural integrity of the product is questionable and not all the material is preserved such that the length measured is only that remaining on the original sample. A portion of those samples were ejected during combustion. At 16 wt% GA, the pellet's length could not be measured because the pellet did not maintain its original structure and was blown apart by convective forces dominating the reaction.

According to Shteinberg et al. [27], there are two main processes associated directly with the volume growth of the sample that can be distinguished in the combustion wave. The first consists of melting of one reactant and capillary flow along the particles of the other components. The second is the decomposition of the gasifying additive. An increase in the gas pressure in the pores of the sample causes them to enlarge and the entire volume of the sample to increase [27]. The elongation depends on the gas pressure in the pores of the sample which can be controlled by varying the amount of gasifying agent in the green mixture. The sample will continue to elongate until a critical amount of gasifying agent is added. At this point, the homogeneity of the sample is debased [27,28]. Fig. 9 shows the maximum point of elongation to occur when the GA reaches 10 wt%. Further addition of GA

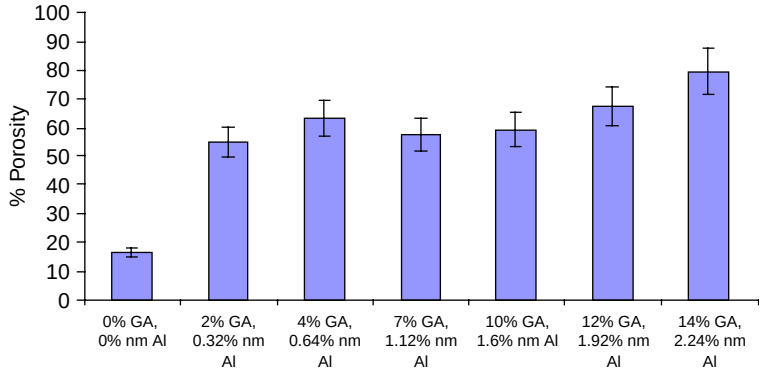

Fig. 7. Porosity as a function of wt% gasifying agent (GA) and nanometer Al (nm Al).

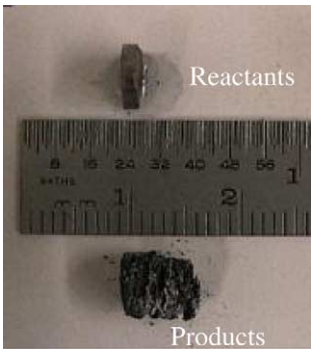

Fig. 8. Elongation of a pellet containing 7 wt% GA and 1.12 wt% nm Al reactant particles.

cause the structure to lose stability and blow apart during combustion.

4. Discussion

4.1. Ignition delay time

The trend in Fig. 5 more likely results from the addition of nm Al particles than from the addition of $C_{13}F_{27}COOH$. Aluminum nanoparticles are more reactive than micron-sized particles in intermetallic reactions as a result of high specific surface area [16].

In a recent study by Moore et al. [29] μm Al particles were incrementally replaced with nm Al particles and combined with a highly exothermic oxidizer, molybdenum trioxide, MoO_3. They showed that adding only 10% nm Al significantly enhanced ignition by reducing the ignition delay time by two orders of magnitude [29]. Other researchers have noted similar reduced ignition delay times through similar bimodal Al particle size distributions reacting with ambient air [30] and as an additive in a propellant (ammonium perchlorate, AP) [31]. However, in [16,29–31] the nm Al particles were passivated with Al_2O_3, whereas in this study, the nm Al particles are passivated with $C_{13}F_{27}COOH$. It was reasoned in [17,29] that Al_2O_3 passivated nm Al particles undergo a completely different ignition mechanism than their μm counterparts, and that this different mechanism explains the increased sensitivity to ignition. The ignition mechanism can be described first by the phase change in the Al_2O_3 passivation shell which is accompanied by a roughly 20% increase in shell density [32]. This phase change exposes the Al core particle at temperatures as low as 350 °C [32], below the bulk melting temperature of Al (660 °C [24]), and corresponds with the ignition temperature of nm Al composites [16,17]. Therefore, nm Al ignition occurs in the solid phase whereas μm Al particles ignite above the Al bulk melting temperature and in the liquid phase. Although the nm Al particles used in this study are passivated with $C_{13}F_{27}COOH$ rather than Al_2O_3, Fig. 5 suggests that adding even small quantities of nm Al particles (i.e. only 2.24 wt%), regardless of the passivation shell enhances the overall mixtures' sensitivity to ignition by reducing ignition delay times by up to two orders of magnitude.

The temperature measurements generally compare the thermal response of the samples and are intended as an estimate for qualitative comparison of temperature as a function of nm Al content. The results indicate that the nm Al particles in excess of 1 wt% trigger a shift in the ignition mechanism from liquid–solid to solid–solid diffusion. This is a significant finding for two primary reasons:

(1) Other studies noted this ignition mechanism shift for nm Al contents at or exceeding 10 wt%, but did not investigate lower weight percentages of nm Al content [29,30,33]. This is the first study to show that ignition behaviors are affected by as little as 1 wt% nm Al content; and
(2) The nm Al particles used in this study are passivated by $C_{13}F_{27}COOH$ and not Al_2O_3, yet the same general ignition temperature behaviors as reported by other researchers are also observed in Figs. 5 and 6 [16,17,21,29,30,33]. This implies that the rate-determining step in nm Al oxidation for Al_2O_3-passivated Al may be triggered at roughly the same temperature as for $C_{13}F_{27}COOH$-passivated Al.

4.2. Combustion velocity

Table 1 indicates that the transition from normal to convective burning corresponds with the addition of GA

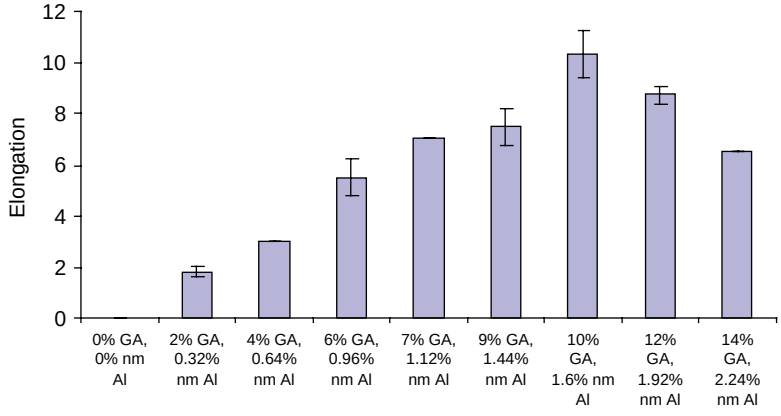

Fig. 9. Elongation ($\Delta L/L_0$) as a function of wt% GA and nm Al content.

which may generate higher pressure gradients inside the pores and facilitate an increase in the rate of gas penetration into the unburned portions of the pellet. The result is a higher combustion velocity and greater porosity (as will be discussed in Section 4.3) in the products. Mathematically, the partial differential equations describing unsteady flow of gases through porous media are nonlinear and inhomogeneous, and no simple closed-formed solutions for specified boundary and initial conditions can be derived [34]. Margolis et al. [35] developed a numerical model to describe the influence of subsurface gaseous combustion on the burning of porous materials. They conclude that the phenomenon referred to as the transition from conductive to convective burning corresponds to an increase in 'overpressure,' the pressure that drives the convective gases into the unburned reactants [36]. They also note that the transition from conduction to convection is further enhanced when the gaseous reaction is allowed to penetrate into the porous solid, due to the fact that the heat release within the subsurface region serves to further preheat the solid material beyond the preheating caused by conduction and pressure-driven convection. This in turn enhances the reaction rate, and hence, the combustion velocity [36].

4.3. Porosity and microstructure of the products

Increasing the porosity of a material will effectively decrease the overall thermal conductivity. The effective thermal conductivity (k_{eff}) is a local volume-averaged conductivity used for reactant matrices along with the assumption of a local thermal equilibrium between the solid, fluid, and gas phases [26]. The effective thermal conductivity is a function of the material, porosity, temperature, and microstructure. Kaviany [26] presents correlations to determine an effective thermal conductivity for given phase distributions of a representative elementary volume, V. Eq. (4) uses the concept of a geometric mean to determine an effective thermal conductivity for porous media [26].

$$\frac{k_{eff}}{k_g} = \left[\frac{k_{max}}{k_g}\right]^{s}\left[\frac{k_{min}}{k_g}\right]^{1-s} \quad (4)$$

In this equation k_{eff} is calculated based on the limiting thermal conductivities of the material, where k_{min} is the minimum thermal conductivity of the material taken to be the Ni (90 W/m K [24]), k_{max} is the maximum thermal conductivity taken to be that of the Al (273 W/m K [24]) and k_g is the thermal conductivity of the gas in the pores (assumed to have properties similar to air at 2000 K). The s in Eq. (4) is described as a wetting parameter and an inverse function of the porosity of the products [26]. Fig. 10 shows the data for effective thermal conductivity based on the porosity measurements and a corresponding power law curve fit.

The thermal conductivity continues to decrease as the porosity of the material increases leading to the improved property of heat resistance for the NiAl alloy. The averaged conductivity term typically used for the NiAl alloy is 194 W/m K [16]. Increasing the porosity from 0 to 16% reduces the thermal conductivity to 97 W/m K and increasing the porosity to 80% further reduces the effective thermal conductivity. These results show that even small increases in the porosity of the final metallic alloy will enhance the thermal resistance properties by a factor of two.

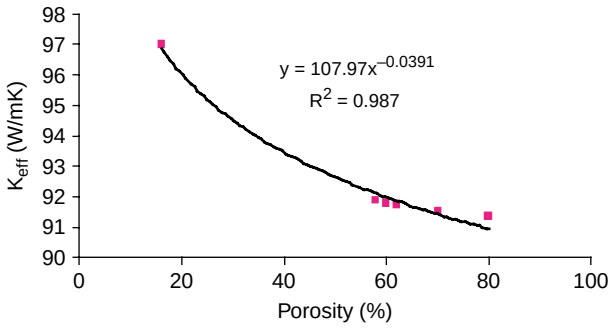

Fig. 10. Effective thermal conductivity as a function of porosity (%).

Nickel aluminides are currently being used as high-temperature, wear-resistant coatings applied to surfaces that experience second- or third-body interactions. Because this alloy has good high temperature and structural properties, the material is ideal for hot turbine sections as well. Continuous development and advancement in thermal barrier coatings is needed due to the increase in gas turbine engine temperatures. Tremendous effort has been devoted to developing new thermal barrier coating materials and processing methods in order to decrease the thermal conductivity [36]. The results from this study are significant because they show the production of a NiAl superalloy that offers the superior hardness inherent from Ni, the oxidation and hot corrosion resistance associated with Al, and a reduction in thermal conductivity by a factor of two resulting form the highly porous product structure. This material could be used as an improved thermal barrier coating in high-temperature gas turbine engines.

5. Conclusions

The formation of a new intermetallic derivative of the traditional NiAl alloy was examined by incorporating nm Al particles passivated with a gasifying agent ($C_{13}F_{27}COOH$) into a reactant recipe of micron-scale Al and nm Ni particles. The reactants were laser ignited and the products formed via self-propagating high temperature synthesis. The unique passivation shell on the nm Al particles resulted in three very significant findings for combustion and product microstructure.

First, it was shown that adding as low at 2.5 wt% nm Al particles to the traditional reactant mixture resulted in reduced ignition delay times by two orders of magnitude. This reduction in ignition delay time was attributed to the increased reactivity of the nm Al particles that appear to be independent of the surface coating. In particular, ignition temperatures were found to correspond to the ignition temperatures of Al_2O_3 passivated nm Al containing thermites, suggesting that the rate determining step for nm Al oxidation mechanism occurs at

roughly the same temperature for Al_2O_3 passivated nm Al as for $C_{13}F_{27}COOH$ passivated nm Al.

Second, the flame propagation behavior was found to shift from a normal diffusive burning to a convectively dominant mechanism at 7 wt% gasifying agent. The transition was determined based on an analysis of the Andreev (*An*) number which is similar to the *Pe* number but tailored to reacting flow through porous media. It was shown that when $An < 0.18$, the flame is propagating under normal diffusive burning conditions and when $An > 0.18$, the mechanism for propagation is controlled by convection.

Third, the porosity of the metallic alloy was shown to increase by roughly a factor of 8 (i.e. from 10 to 80% porosity for 0–14 wt% gasifying agent). This significant increase in porosity translates to a significant reduction in thermal conductivity. In fact, increasing the porosity to 80% reduces the effective thermal conductivity by a factor of two (i.e. 194–91 W/m K). The reduction in thermal conductivity based upon increased porosity has significant implications for industrial applications. For example, porous nickel aluminides maintain the superior hardness properties inherent from Ni and the oxidation and hot corrosion resistance properties associated with Al, but with a reduction in thermal conductivity the alloy has potential as an effective thermal barrier coating in high-temperature and corrosive applications such as for gas turbine components.

Acknowledgements

M.L. Pantoya and E.M. Hunt would like to gratefully acknowledge support from the Army Research Office under grant number W911NF-04-1-0217. We are also thankful for support provided by the National Science Foundation under grant number CST-021014 and our program manager, Dr Linda Blevins.

References

[1] Alvin MA. Impact of char and ash fines on porous ceramic filter life. Fuel Process Technol 1998;56(1–2):143–68.
[2] Aldushin AP, Rumanov IE, Matkowsky BJ. Maximal energy accumulation in a supoeradiabatic filtration combustion wave. Combust Flame 1999;118(1–2):76–90.
[3] Poladi RH, Landry CC. Oxidation of octane and cyclohexane using a new porous substrate, Ti-MMM-1. Microporous Mesoporous Mater 2002; 52(1):11–18.
[4] Gobina EN, Oklany JS, Hughes R. Elimination of ammonia from coal gasification streams by using a catalytic membrane reactor. Ind Eng Chem Res 1995;34(11):3777–83.
[5] Ayers RA, Thorne K, Moore JJ, Schowengerdt F. Combustion synthesis of porous materials for bone replacement. Biomed Sci Instrum 2001;37: 463–8.
[6] Ayers RA, Zhang X, Schowengerdt F, Moore JJ. Combustion synthesis of porous materials for bone replacement. Biomed Sci Instrum 2001;37: 469–74.
[7] Borovinskaya IP, Merzhanov AG, Uvarov VI. SHS materials of graded porosity. Mater Sci Forum 1999;308:151–6.
[8] Zhou W, Hu WB, Zhang D. Combustion synthesis of highly porous ceramics: the TiC–Al_2O_3 system. J Mater Sci 1999;34(18): 4469–73.
[9] Shcherbakov VA, Merzhanov AG. Structure formation in porous materials produced by gravity-sensitive SHS. Combust Sci Technol 1998;136:253–77.
[10] Reiss H, Wilson IB. The effect of surface on melting. J Colloid Sci 1948; 3:551–61.
[11] Wronski CRM. The size dependence of the melting point of small particles of tin. Br J Appl Phys 1967;18:1731–7.
[12] Yang Y, Wang S, Sun Z, Dlott DD. Propagation of shock-induced chemistry in nanoenergetic materials: the first micrometer. J Appl Phys 2004;95(7):3667–76.
[13] Licheri R, Roberto O, Giacomo C. Chemically-activated combustion synthesis of TiC–Ti composites. Mater Sci Eng A 2004;367(1–2):185–97.
[14] Dyatlova EM, Gailevich SA, Minenkova GY, Radchenko SL. High-melting heat-insulating materials obtained by foaming and gassing methods. Glass Ceram 2002;59(1–2):57–60.
[15] Varma A. Form from fire. Sci Am 2000;August:58–61.
[16] Hunt E, Plantier K, Pantoya M. Nano-scale reactants in the self-propagating high-temperature synthesis of nickel aluminides. Acta Mater 2004;52(11):3183–91.
[17] Hunt EM, Pantoya ML. Ignition dynamics and activation energies of metallic thermites: from nano– to micron–scale particulate composites. J Appl Phys; 2005;98:034909–17.
[18] Munir ZA, Anselmi-Tamburini U. Self-propagating exothermic reactions: the synthesis of high temperature materials by combustion. Mater Sci Rep 1989;3:277–365.
[19] Merzhanov AG. Theory and practice of SHS: worldwide state of the art and the newest results. Int J Self Propag High Temp Synth 1993;2(2): 113–1158.
[20] Shteinberg AS, Shcherbakov VA, Merzhanov AG. Self-propagating high temperature synthesis of high-porosity materials under zero-*g* conditions. Transl Dokl Akad Nauk SSSR 1991;318(2):337–41.
[21] Granier JJ, Pantoya ML. Laser ignition of nanocomposite thermites. Combust Flame 2004;138:373–83.
[22] Granier JJ, Plantier KB, Pantoya ML. The role of the Al_2O_3 passivation shell surrounding nano-aluminum particles in the combustion synthesis of NiAl. J Mater Sci 2004;39:1–11.
[23] Jouet RJ, Warren AD, Rosenberg DM, Bellitto VJ, Park K, Zachariah MR. Surface passivation of bare aluminum nanoparticles using perfluoroalkyl carboxylic acids. Chem Mater 2005;17:2987–96.
[24] Weast RC, editor. CRC handbook of chemistry and physics. 64th ed. Boca Raton, FL: CRC Press; 1984.
[25] Bobolev VK, Margolin AD, Chuiko SV. Stability of normal burning of porous systems at constant pressure. Combust Explos Shock Waves 1966; 2(4):24–32.
[26] Kaviany M. Principles of heat transfer in porous media. New York: Springer; 1991.
[27] Shteinberg AS, Shcherbakov VA, Martynov VV, Mukhoyan MZ, Merzhanov AG. Self-propagating high-temperature synthesis of high-porosity materials under weightlessness. Sov Phys Dokl 1991;36(5).
[28] Shcherbakov VA, Merzhanov AG. Self-propagating high-temperature synthesis of cermet foam material. Transl Dokl Akad Nauk 1997;354(3): 346–9.
[29] Moore K, Pantoya ML, Son SF. Combustion behaviors resulting from bimodal aluminum size distributions in thermites. J Prop Power; in press.
[30] Popenko EM, Il'in AP, Gromov AM, Kondratyuk SK, Surgin VA, Gromov AA. Combustion of mixtures of industrial aluminum powders with superfine powders of aluminum and aluminum oxide in air. Combust Explo Shock Waves 2002;38(2):157–62.
[31] Dokhan A, Price EW, Seitzman JM, Sigman RK. The effects of bimodal aluminum with ultrafine aluminum on the burning rates of solid propellants. Proc Combust Inst 2002;29(2):2939–45.
[32] Trunov MA, Schoenitz M, Zhu X, Dreizin EL. Effect of polymorphic phase transformations in Al_2O_3 film on oxidation kinetics of aluminum powders. Submitted for publication.

[33] Hunt EM, Granier JJ, Plantier KB, Pantoya ML. Nickel aluminum superalloys created by the self-propagating high-temperature synthesis (SHS) of nano-particle reactants. J Mater Res 2004;19(10):1–9.
[34] Kuo KK, Vichnevetsky R, Summerfield M. Theory of flame front propagation in porous propellant charges under confinement. AIAA J 1972;11(4).
[35] Margolis SB, Telengator AM, Forman AW. Influence of subsurface gaseous combustion on the burning of confined porous energetic materials. Combust Sci Technol 2003;175:421–52.
[36] Wang D, Huang X. Design of a multiple layered thermal barrier coating structure for optimized thermal properties. Second international symposium on aerospace materials and manufacturing.